C. R. Physique 13 (2012) 328–336

Contents lists available at SciVerse ScienceDirect

Comptes Rendus Physique

www.sciencedirect.com

Use of large scale facilities for research in metallurgy

Bulk evaluation of ductile damage development using high resolution tomography and laminography

Evaluation en volume du développement de l'endommagement ductile par l'utilisation de la tomographie à haute résolution et de la technique de laminographie

Eric Maire [a,*], Thilo Morgeneyer [b], Caroline Landron [a], Jerome Adrien [a], Lukas Helfen [c]

[a] *Universite de Lyon, INSA-Lyon, MATEIS CNRS UMR 5510, 7, avenue Jean-Capelle, 69621 Villeurbanne, France*
[b] *Mines ParisTech, centre des materiaux, CNRS UMR 7633, BP87, 91003 Evry cedex, France*
[c] *ANKA/Institute for Synchrotron Radiation, Karlsruhe Institute of Technology, Karlsruhe, Germany*

ARTICLE INFO

Article history:
Available online 27 January 2012

Keywords:
X-ray
Tomography
Laminography
Damage
Fracture
Ductile

Mots-clés :
Rayons X
Tomographie
Laminographie
Endommagement
Rupture
Ductile

ABSTRACT

Ductile fracture of metals is accompanied at the microscopic scale with the appearance of damage, in the form of small cavities. Damage progress is divided into three distinct and consecutive phases: initiation, growth and coalescence. This article illustrates the use of three-dimensional nondestructive imaging to study this damage development. Two techniques, mainly based on the attenuation of X-rays are now used for this type of studies at high resolution: tomography and laminography. The interest of laminography is that samples with larger dimensions (in the form of sheets) than the conventional tomography ones can be used. Examples of images obtained with the two techniques, as well as quantification using X-ray tomography, are presented.

RÉSUMÉ

La rupture ductile des métaux est accompagnée du processus microscopique d'apparition d'endommagement, sous forme de cavités de dimension micronique. Cet endommagement est décomposé en trois phases distinctes et consécutives : l'amorçage, la croissance puis la coalescence. Cet article recense et illustre l'utilisation de l'imagerie tridimensionnelle non destructive pour l'étude microscopique de cet endommagement. Deux techniques basées sur l'absorption des rayons X sont maintenant utilisables à haute résolution : la tomographie et la laminographie. La laminographie présente l'intérêt d'autoriser l'utilisation d'échantillons de grandes dimensions (plaques) comparées aux petites éprouvettes de tomographie habituelles. Des exemples d'images obtenues à l'aide de ces deux techniques ainsi que les méthodes de quantification de l'endommagement par traitement d'image dans la cas de la tomographie sont présentés.

* Corresponding author.
E-mail address: eric.maire@insa-lyon.fr (E. Maire).

1631-0705/$ – see front matter
doi:10.1016/j.crhy.2011.12.009

1. Introduction

Improving the performance of structural materials is of particular technological importance. This improvement has been a long lasting driving force in the field of materials science, especially as far as the fracture properties of materials are concerned. The rupture of materials, metals in particular in the present paper, is a rather complex process which has drawn a lot of attention during the last decades. The purpose of the most recent studies is to describe the physics and mechanics of the fracture process in as much detail as possible. The most promising methods to model fracture are indeed those taking the microstructure of the material into account. Ultimately, the aim is to use microstructure optimization as a tool to delay fracture. These methods all rely on a sound characterization of the microstructure and on a reliable observation of the damage mechanisms. A better knowledge of these mechanisms will guide the modeling efforts. It will then be possible to directly compare measurements performed at the scale of the micro-damage events with results from calculations at the local scale.

Using standard microscopy methods, it has been shown experimentally decades ago that ductile deformation is accompanied with the formation of micro-damage in the form of small sized voids leading to the final fracture. Damage development during the straining of a plastic matrix involves void nucleation [1–3], growth [4–6] and coalescence [6–11]. The Beremin approach [12] is a simple way to predict nucleation although more phenomenological models also exist [13]. Cavity growth is a micro-mechanical problem studied in detail in the literature. Models in this field are generally separated into so-called "uncoupled approaches" (Rice–Tracey type [14]) and "coupled approaches" (Gurson type [15]). The coalescence remains the most difficult phase to study experimentally and to predict. Two models are commonly used, i.e. the geometrical approach proposed by Brown and Embury [16] and the micro-mechanical framework of Thomason [11]. Apart from a few studies [17, 18], a lack of quantitative experimental data on industrial materials for these different steps has limited the development of physically based models for the failure prediction of metals. Numerical models that take into account these three steps have been proposed by Worswick et al. in the literature [19], but these models have only once [20] been validated by comparing results with bulk observations.

One of the best solutions available today to observe changes in the microstructure due to damage is High Resolution X-ray Computed Tomography (HRXCT) [20–24]. This technique can be used like a simple microscopy technique with a resolution on the order of 1 micron. The method provides a different type of information in the form of three dimensional (3D) nondestructive images of the bulk of the observed material. A number of findings have been clearly established during the last decade using this new method. Precise quantitative measurements of the different phases involved in damage evolution (initiation, growth and coalescence of cavities) have been achieved for model aluminum matrix materials [21] and for steels [22], each time leading to an improvement in the modeling and each time showing that surface quantification could lead to a large underestimation of the quantity of damage compared to the amount actually present in the bulk of the sample.

One of the limits of the HRXCT method is that the sample is restricted in size with respect to the two directions perpendicular to the rotation axis. With recent advances in synchrotron radiation (SR) imaging techniques it has become possible to perform three-dimensional (3D) imaging of objects that are thin but extended in two directions [25]. This relatively new method, High Resolution X-ray Computed Laminography (HRXCL) [26], allows for imaging of thin sheet materials in terms of constituent phases. This opens doors for observation of damage processes during in situ loading of sheets. Damage evolution ahead of a crack in composite laminates has been successfully observed using HRXCL in similar resolution as typically obtained by HRXCT [27,28]. For metal alloy sheet materials, that are e.g. aluminum alloy sheets for aerospace [29], automotive or packaging applications or steel sheets for automotive applications [30], the possibility now arises to perform in situ experiments that allow to follow the damage evolution within the material. As such, tensile experiments on smooth or notched tensile or butterfly specimens [30] can be performed in situ and the evolution of deformation and damage can be followed within the material. In particular, ductile crack initiation and propagation ahead of notches/cracks can now be studied in thin sheet metals using test specimens with sizes and geometries that are similar to configurations found in typical engineering applications of the structural material. The observation zone sampled during one scan remains of the same typical size compared to HRXCT, but the reconstruction restrictions leading to the cutting of small samples vanish and one can work using large scale sheets. Small specimen size can for instance become a problem when the plastic zone size around the notch becomes larger than the specimen size. In this situation laminography is superior compared to in situ tomography [31].

This article reviews our own recent experimental results using X-ray tomography and laminography to evaluate the evolution of ductile damage in the bulk of metals. We divided the paper into two distinct parts, one for tomography and one for laminography. In each of these parts, we report the qualitative nature of the observations made and we show how these open new possibilities for measuring damage and comparing it to damage prediction by standard models.

2. Synchrotron tomography

2.1. Experimental setup

It is not the purpose of the present paper to describe the tomography technique in detail. Many preceding papers have been published and can be referred to (see, for instance, the review in [32]). The current issue of the journal in which this

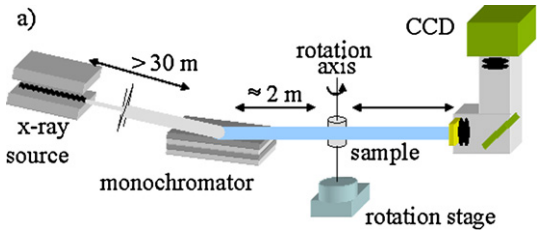

Fig. 1. Schematic description of synchrotron CT.

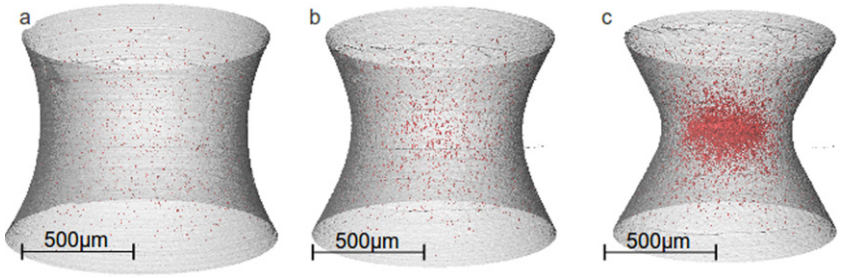

Fig. 2. 3D views of a notched strained specimen at various steps of deformation: (a) $\varepsilon_{loc} = 0$; (b) $\varepsilon_{loc} = 0.35$; and (c) $\varepsilon_{loc} = 0.83$. The outline of the specimen appears in gray and the cavities in red.

paper is included also contains many papers related to tomography. We use standard high resolution tomographs located on synchrotron beam lines, mainly ID19 and ID15 at the ESRF. A typical setup used on ID19 for acquiring the radiographs necessary for reconstructing a 3D image of the sample in synchrotron tomography is shown in Fig. 1. Later in the paper, it will be possible to compare this setup and the one used for laminography.

2.2. Qualitative results

Qualitative images of the development of ductile damage during in situ tensile testing of metals have been published widely in the literature. One of the first examples was the visualization of the cracking of particles in model aluminum matrix composites containing very large SiC angular particles in [33]. Model composites containing spherical particles were then studied in [21,34]. The choice of these model systems was dictated by the relatively new character of the technique, that still needed validation for this type of studies at that time. Studies on actual industrial materials, with a rather simple microstructure, were then performed starting with Ti composites reinforced with large size monofilament SiC fibers [35]. In parallel, low absorbent industrial aluminum alloys were also investigated using this method for example in [36]. Contrarily to the model materials initially tested, in this last example, the cavities and the microstructure to image were rather small, and the imaging part, achieved at a voxel size of 0.7 or 0.3 µm was a challenge. In these materials with a complex microstructure, the shape of the developed cavities was also rather complex. More recently in situ tensile tests have been applied to more absorbent materials such as steels [22], copper [23], titanium [37] and cobalt [38]. Fig. 2 shows a recent example obtained on a steel notched sample. This dual phase steel was imaged during an *in situ* tensile test and the figure shows three of the many different deformation steps applied to the sample (a, b and c correspond to strains of 0, 0.35 and 0.83 in the figure, respectively). The figure shows that the method is able to describe precisely the outer shape of the sample, seen as a transparent surface in the figure. This description of the shape is used, as explained in the next section, to measure some macroscopic mechanical parameters and their evolution during the test. Fig. 3 also shows gray level reconstructed slices extracted from the middle part of the sample at the same value of the strain. The tensile axis is vertical in these figures. It can be clearly seen that during the tensile test, cavities nucleate, grow and then coalesce. These three main steps can then be analyzed separately using these images. This remains one of the main strength and interest of the method for the study of ductile damage.

2.3. Quantification

Damage can for instance fully be quantified according to a procedure already presented in [22]: a little sub-region of the reconstructed sample is followed at each deformation step. The sub-region is a cubic volume of $(300\ \mu m)^3$ located exactly in the middle of the region where the section of the sample is the smallest. This section remains the same in the sample before and after necking. This sub-volume is the region undergoing the highest triaxiality and the highest strain during the tensile test. The size has been chosen sufficiently large to be representative but also sufficiently small to assume that strain and stress triaxiality are almost constant inside the volume. The knowledge of the section S of the sample allows us to estimate the true value of the total strain in the sub-volume by the following expression:

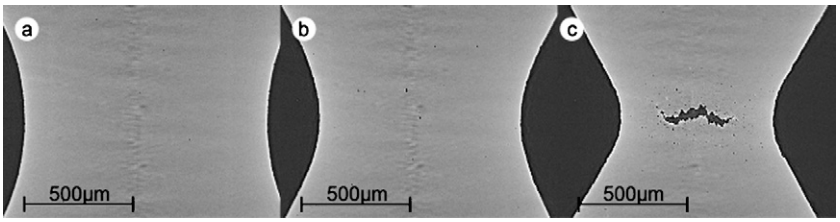

Fig. 3. Sections at the center of a notched strained specimen at various steps of deformation: (a) $\varepsilon_{loc} = 0$; (b) $\varepsilon_{loc} = 0.35$; and (c) $\varepsilon_{loc} = 0.83$.

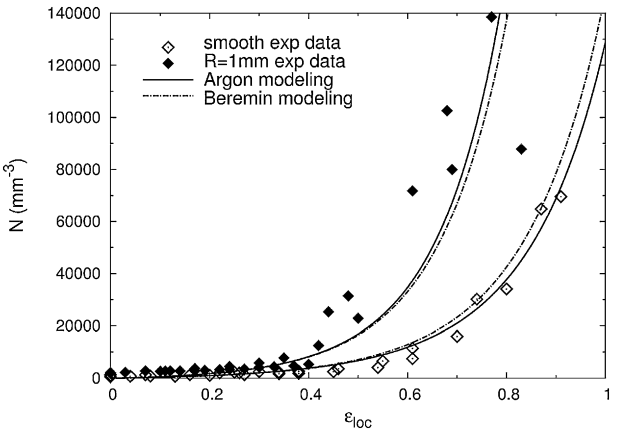

Fig. 4. Comparison of the predictions of the nucleation models based on the Argon criterion and the Beremin criterion, and the experimental data on 11% DP steel.

$$\varepsilon = \ln \frac{S_0}{S}$$

where S_0 is the initial section. It has been shown by FE simulation that the spatial fluctuation of the strain over this little sub-volume was less than 4% so assuming that it is constant is close to reality. The force F also recorded during the tensile test is used to calculate the true stress:

$$\sigma = F/S$$

The radius of curvature of the notch can also be easily measured and then be used to assess the triaxiality so that all the mechanical parameters important for damage calculation are known at each deformation step.

The sub-region is filtered and thresholded using standard 3D image processing methods. Each pore is then labeled and morphological parameters can be directly measured and used as explained below to analyze nucleation, growth and coalescence independently.

2.3.1. Nucleation

Nucleation can be straightforwardly quantified by counting the number of cavities in the sub-volume. It is only affected by coalescence in the end of the test where sometimes, the number of cavities per cubic millimeter can be measured to decrease (see Martin et al. [39] for an example during superplastic deformation). Fig. 4 shows for instance that nucleation is extensive in DP steels at high strain. The figure also shows that for the notched samples the nucleation occurs at a smaller strain than for the smooth sample, comforting the generally admitted idea that nucleation is promoted at higher stress triaxiality.

The lines in the figure are the result of two different models predicting the evolution of the amount of nucleation with strain. The first model is the classical Beremin approach of nucleation based on the calculation of the stress inside the particles. The second model was presented in [40] and is based on a slightly different micro-mechanical calculation of the stress at the interface between ferrite and martensite. Both models contain some unknown parameters (like for instance the strength of the interface) that have to be fitted. The fit was performed using the experimental data of the smooth sample in each case. Both models were then blindly run using these fitted parameters to predict the evolution of nucleation in the notched specimen. It can be seen on the figure that the prediction of both models is in good agreement with the experimental measurement. As a consequence these two approaches are identified in our study as easy to implement and efficient ways for the prediction of damage in these materials.

2.3.2. Growth

Quantifying growth is straightforward when the cavities are rather large and not in a too large number inside the reconstructed block to be analyzed. This has then mainly been achieved so far using model materials. One of the first examples of measurement using X-ray tomography was published in [34]. The sample in this case was made of a model composite for which each cavity was easy to follow manually. The second chronological example can be found in [23] where large (50 µm in diameter) holes where pre-drilled in thin (50 µm in thickness) metal sheets. These pre-drilled sheets were subsequently diffusion bonded to create a bulk pre-damaged sample in which the nucleation step was short circuited because the cavities were already present. In this case, growth could easily be followed and successfully compared with the Rice and Tracey model.

For industrial materials, like for instance in the case of the DP steel shown in Fig. 2, growth quantification proved to be more tedious because it was practically very difficult to track each cavity from one deformation step to the next. A pragmatic alternative approach was then adopted in [22] where the N largest cavities of the population were assumed to remain the same at each deformation step. Measuring the average size of these N largest cavities was much easier and this allowed us to fit the parameters of the Rice and Tracey model for growth to the experimental observation.

2.3.3. Coalescence

Very little has been achieved so far in the literature in terms of quantification of the coalescence phase using X-ray imaging. The work of Weck et al. [23], on model materials using in situ small size tensile samples, still remains the only example where coalescence was quantified at the microscopic level and the two classical prediction models (i.e. Brown and Embury [16] and Thomason [11]) were compared with experiments. The study showed that the later Thomason's model is a mechanical framework of wider applicability and can be used with success for both plane strain and plane stress states on the model materials studied. Work is in progress for trying to identify and validate these two models at a microscopic scale using the experimental results obtained on industrial materials. Our first (still unpublished) measurements made by identifying the couples of closest cavities just prior to fracture seem to indicate that the general picture used in the model where the two coalescing cavities have their centers in a plane perpendicular to the tensile axis is far from representing the actual situation. For industrial materials in the form of sheets, coalescence can be divided into two kinds of mechanisms: (1) coalescence by impingement at high levels of stress triaxiality; and (2) coalescence by void sheeting dominated by shear deformation at lower levels of stress triaxiality. The underlying physics of both mechanisms are to date still poorly understood. Further observations and quantifications of both mechanisms is necessary to obtain better models.

2.4. Recent improvements

The recent improvements of the tomography technique consisted in a substantial reduction of the temporal and the spatial resolution. This section highlights the use of these recent improvements in the field of the investigation of ductile damage.

2.4.1. Continuous experiments

For a long time, HRXCT has required a long exposure time for collecting the radiographs in a number sufficiently large to allow a good reconstruction. In year 2004, 10 minutes was a minimum to record a scan and perform a good quality reconstruction. This has led us to achieve most of our early work using a mode where we stopped the displacement of the tensile grip and maintained it at a fixed value during the acquisition. Most of the results mentioned in the previous part of this paper were achieved in this so-called "interrupted *in situ*" mode. Recent advances in the detector technology for imaging have allowed us to reduce drastically the time required to record a scan. This has allowed us to recently perform continuous *in situ* tensile tests. The first example was published in [41].

It is worth comparing the impact of these different procedures on the quantitative measurement of damage. Fig. 5a shows the comparison of this quantification using both types of procedures (interrupted and continuous) for the nucleation process (density of cavities). Fig. 5b shows the same comparison for the growth phase measured here by means of the evolution of the average diameter of the largest cavities in the studied population. These figures demonstrate that in the particular case of the DP11% material, the quantification can be performed using the continuous in situ acquisition mode without a significant error despite the reduced quality of the images in this mode, especially as far as the size of the cavities is concerned. The density of cavities is only slightly smaller in the continuous in situ mode, probably because the smallest pores are ignored by the image processing procedure applied, owing to the slightly lower quality of the images. The conclusion drawn for this particular material, already made for model composites in [41] shall not be extended to other systems without due consideration. Materials sensitive to strain history and to viscous effects might behave differently.

2.4.2. Very high resolution

The quantitative results concerning the nucleation step are particularly sensitive to the resolution at which the images are acquired. This has been mentioned in the preceding section where less voids were counted when the image quality was reduced for obtaining a faster acquisition. This was also previously directly shown in [42]. The nucleation of cavities quantified using X-ray tomography can only be considered as a lower limit and there are probably voids smaller than the resolution power of the tomograph used. This is generally neglected as the cavities leading to the final fracture are, in

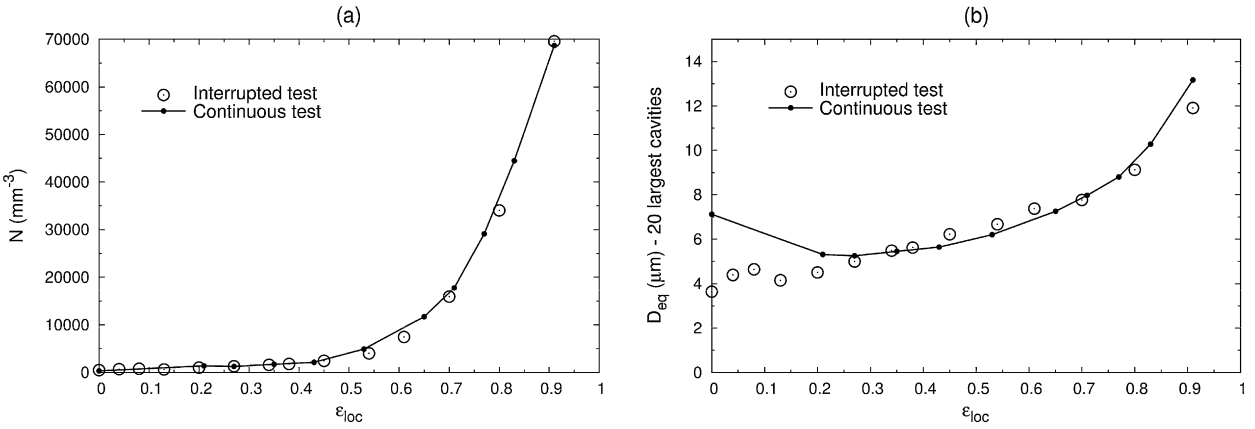

Fig. 5. Comparison of the experimental data acquired during interrupted test and continuous test: (a) data concerning void nucleation; (b) data concerning void growth.

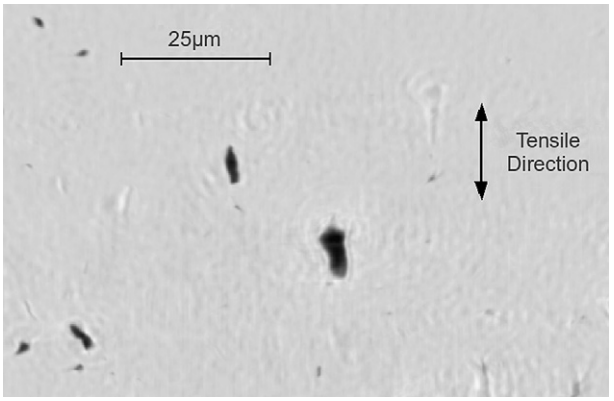

Fig. 6. Cross section inside the tomography volume of a DP steel acquired with a voxel size of $100 \times 100 \times 100$ nm^3.

practice, the larger ones of the population. There are however cases where a very high resolution is needed. This appears when the initial microstructure of the material to be tested has a small scale. The dual phase steels shown in Fig. 6 are good examples where cavities are small and imaging these with a higher resolution leads to an increase in the number of cavities detected.

Very high resolution in X-ray tomography can now be achieved using Kirkpatrick–Baez mirror devices on synchrotron tomographs. This is for instance routinely achieved at the ESRF on beamline ID22-NI. Examples of high resolution reconstruction of engineering materials can for instance be found in [43]. We have recently used this beamline to analyze the population of nucleated cavities in the same DP steel as is shown in Fig. 2. A tomography slice reconstructed with a voxel size of 100 nm is shown in Fig. 6. Black cavities of very small size can be seen in this reconstruction. Future work will focus on the quantification of these images and the use of this high resolution version of the technique to follow the evolution of a same population of cavities at different values of plastic strain during an ex situ tensile test.

3. Laminography

3.1. Details on the experimental technique

Originally, HRXCL was developed for high-resolution nondestructive device testing [44,45] of small batches of devices, e.g. from early production or testing cycles. Due to established 2D production and integration techniques, flat and laterally extended specimens are predominant in microelectronics and microsystem technology.

Apart from the high spatial resolution which can be achieved for reasonable scanning times due to the high X-ray flux, the application of synchrotron radiation brings additional opportunities, for example an imaging mode called phase contrast [46,47] based on Fresnel diffraction. This enables weakly absorbing specimens or specimen structures to be investigated by laminographic imaging [48,28] which opens up new application fields in materials science [27,28].

HRXCL allows 3D imaging of a limited region of interest (ROI) out of a specimen which is extended larger than the field of view in two dimensions (away from the rotation axis). The third dimension (i.e. the thickness) should be in the order of the field of view of the detector. The acquisition geometry of SR tomographic imaging is shown in Fig. 7 (cf. HRXCT

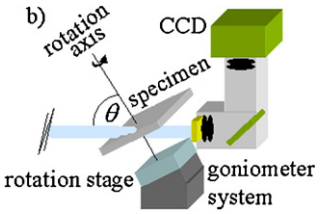

Fig. 7. Schematic description of HRXCL.

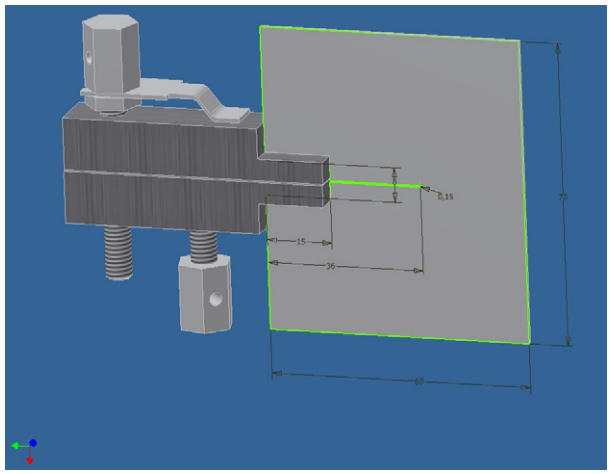

Fig. 8. Loading rig and in situ specimen (dimensions in mm, thickness 1 mm).

of Fig. 1). HRXCL can be considered as a generalization of HRXCT where the tomographic rotation axis is perpendicular to the transmitted beam ($\theta = 90°$) while in HRXCL an angle as close as possible to the surface is chosen where still reliable projection data can be acquired from the flat specimen. Due to the missing information from angles almost parallel to the specimen surface, laminographic imaging is inherently afflicted by imaging artefacts in comparison to CT performed on standard (e.g. cylindrical as in Fig. 1) samples. Applying limited-angle CT to flat specimens, however, such missing projections are prone to generate other imaging artefacts which can, depending on the specimen, occult its structure and important features of interest [26].

3.2. Example: In situ HRXCL of ductile crack initiation and propagation

In the following, some initial results of the HRXCL observation of ductile crack initiation and propagation in a ductile aluminum alloy sheet for aerospace application are given.

3.2.1. The in situ loading rig

The in situ imaging experiments were carried out at ANKA's microlaminography instrument installed at beamline ID19 of the ESRF. For stepwise *in situ* loading and HRXCL scanning of the crack propagation, the setup shown in Fig. 8 has been used. The setup has a very similar design as the one used in [27]. A specimen with a size of 60 mm × 70 mm × 1 mm with a machined notch with a radius at the notch tip of 0.15 mm is used. The used material is a 2139 alloy for aerospace application in naturally aged (T3) condition. The reader is referred to [18] for further details on the material microstructure and its mechanical behavior. For in situ loading, a wedging device is used where 2 screws allow us to incrementally open the wedge and control the crack mouth opening displacement. About 20 loading steps have been applied and observed via HRXCL.

3.2.2. Qualitative results

Figs. 9a to 9c show some initial results of the crack initiation observed via in situ HRXCL. Reconstructed 2D sections in the sheet plane are shown in a region close to the notch and about 150 µm away from the sheet mid-thickness. The material microstructure can clearly be discerned with initial porosity (in black), intermetallic particles (in white) and the aluminum matrix (in gray) in similar resolution as for HRXCT [48,49]. Relatively strong phase contrast fringes outline the material interfaces between metal and voids. Also, specific laminography artifacts can be seen in these reconstructions but they do not preclude a good visualization of the microstructure. Fig. 9a shows the initial as received material without load containing a cluster of intermetallic particles/voids. The machined notch can clearly be seen. The next loading step is shown

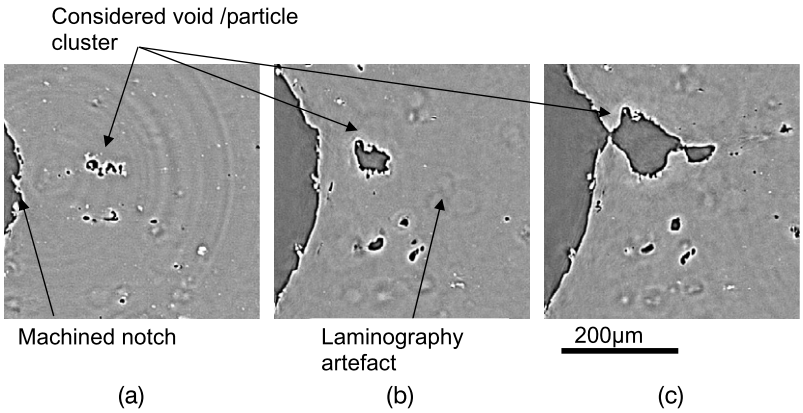

Fig. 9. 2D sections of reconstructed laminography data of an 2139 T3 Al alloy sheet around the machined notch in the crack initiation region and at 150 µm from the sheet mid-plane of (a) the as-received material, (b) at CMOD = 1.75 mm, (c) at CMOD = 2.0 mm.

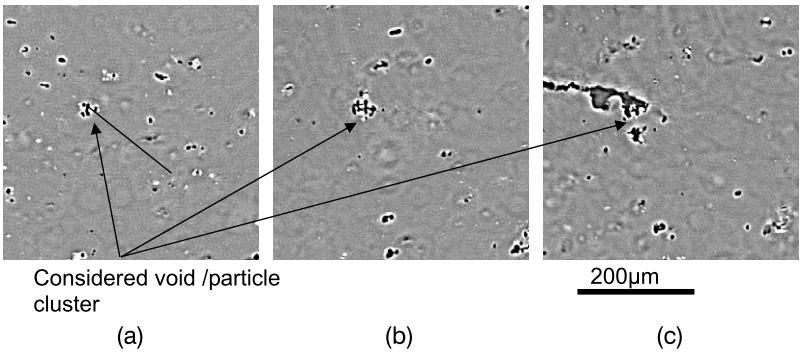

Fig. 10. 2D sections of reconstructed laminography data of an 2139 T3 Al alloy sheet 700 µm from the notch in the crack propagation region and at 330 µm from the sheet mid-plane of (a) the as-received material, (b) at CMOD = 2.25 mm, (c) at CMOD = 2.5 mm.

at a CMOD of 1.75 mm (Fig. 9b) and particle cracking and as well as void growth can clearly be seen. In the following loading step (Fig. 9c) the void has grown further and coalesced with the notch.

In contrast, Fig. 10 shows the evolution of a stringer of voids and intermetallic particles in the crack propagation region about 700 µm from the machined notch and about 330 µm from the specimen mid-thickness. In this location the stress triaxiality ratio is known to be substantially lower than at crack initiation [17]. In Fig. 10a the initial particle/void stringer in the as-received material is shown. The fracture of the particle/void stringer can be seen in Fig. 10b. After some void growth, that is however substantially lower than at crack initiation, the crack and void link up. The crack at this location clearly contains smaller dimples/voids compared to the preceding figure.

4. Conclusion

HRXCT and its extension to HRXCL for sheet samples, allow one to gain insight into fracture mechanisms at different stages of damage evolution involving different levels of stress-triaxiality and, consequently, induced void growth. Typical flat to slant fracture bifurcation may be studied experimentally in three dimensions. Actual measurements of void growth can be carried out for different load steps and different stages of crack propagation. Critical void volume fraction to coalescence or crack mouth opening displacement (CMOD) may now be determined. Although not discussed nor illustrated in this paper, the 3D deformation field can be obtained via Digital Volume Correlation [50] of the 3D images for different load steps. The direct imaging experiments described in the present paper in their very high resolution version are complementary to Small Angle Neutron or X-ray Scattering from which statistical properties concerning nucleation, growth and coalescence of voids can be analyzed. The diffusion signal is indeed modified by the population of small cavities. This has been discussed for precipitation already [51] but remains scarce (except in [52] and [53]) in the field of cavities inside a metal matrix. The obtained in situ data can provide useful input and validation data for existing models for ductile fracture. Hopefully, the large amount of 3D information and the evolution of damage in 3D will stimulate and give rise to new theories on fracture, especially at lower levels of stress triaxiality.

Acknowledgements

The authors wish to thank F. Xu for help with the laminography data evaluation, T. Baumbach for support of the laminography set-up and the ESRF staff of beamlines ID19 (E. Boller) and ID15 (M. Di Michiel) for help and assistance during the synchrotron experiments.

References

[1] S. Goods, L. Brown, Acta Metall. 27 (1979) 1–15.
[2] G. LeRoy, J.D. Embury, G. Edwards, M.F. Ashby, Acta Metall. 29 (1981) 1509–1522.
[3] A.S. Argon, J. Im, R. Safoglu, Metall. Trans. A 6 (1975) 825–837.
[4] K.E. Puttick, Philos. Mag. 4 (1959) 964–969.
[5] S. Floreen, H. Hayden, Scripta Metall. 4 (1970) 87–94.
[6] T.B. Cox, J.R.J. Low, Metall. Trans. 5 (1974) 1457–1470.
[7] A. Thompson, Metall. Trans. A 18 (1987) 1877–1886.
[8] J. Knott, Met. Sci. (1980) 327–336.
[9] I.G. Park, A.W. Thompson, Acta Metall. 36 (1988) 1653–1664.
[10] B. Marini, F. Mudry, A. Pineau, Eng. Fract. Mech. 22 (1985) 989–996.
[11] P. Thomason, J. Inst. Met. 96 (1968) 360–365.
[12] F.M. Beremin, Cavity formation from inclusions in ductile fracture of A508 steel, Metall. Trans. A 12 (1981) 723–731.
[13] C.C. Chu, A. Needleman, J. Eng. Mater. Technol. 102 (1980) 249–256.
[14] J.R. Rice, D.M. Tracey, J. Mech. Phys. Sol. 17 (1969) 201–217.
[15] A.L. Gurson, J. Eng. Mater. Technol. 99 (1977) 2–15.
[16] L.M. Brown, J.D. Embury, in: Proc. 3rd Int. Conf. Strength of Metals and Alloys, Institute of Metals, London, 1973, pp. 164–168.
[17] F. Bron, J. Besson, A. Pineau, Mater. Sci. Eng. A 380 (2004) 356–364.
[18] T.F. Morgeneyer, J. Besson, H. Proudhon, M.J. Starink, I. Sinclair, Acta Mater. 57 (2009) 3902–3915.
[19] M.J. Worswick, Z.T. Chen, A.K. Pilkey, D. Lloyd, S. Court, Acta Mater. 49 (2001) 2791–2803.
[20] O.S. Orlov, M.J. Worswick, E. Maire, et al., J. Eng. Mater. Techol. ASME 131 (2) (2009), Article Number 021001.
[21] L. Babout, E. Maire, R. Fougères, Acta Mater. 52 (2004) 2475–2487.
[22] E. Maire, O. Bouaziz, M. Di Michiel, C. Verdu, Acta Mater. 56 (2008) 4954–4964.
[23] A. Weck, D. Wilkinson, E. Maire, H. Toda, Acta Mater. 56 (12) (2008) 2919–2928.
[24] J.Y. Buffière, E. Maire, J. Adrien, J.P. Masse, E. Boller, Exp. Mech. 50 (2010) 289–305.
[25] L. Helfen, T. Baumbach, P. Mikulík, D. Kiel, P. Pernot, P. Cloetens, J. Baruchel, Appl. Phys. Lett. 86 (2005) 071915.
[26] L. Helfen, A. Myagotin, P. Mikulík, P. Pernot, A. Voropaev, M. Elyyan, M. Di Michiel, J. Baruchel, T. Baumbach, On the implementation of computed laminography using synchrotron radiation, Rev. Sci. Instrum. 82 (2011) 063702.
[27] A.J. Moffat, P. Wright, L. Helfen, T. Baumbach, G. Johnson, S.M. Spearing, I. Sinclair, Scripta Mater. 62 (2010) 97–100.
[28] F. Xu, L. Helfen, A.J. Moffat, G. Johnson, I. Sinclair, T. Baumbach, J. Synchrotron Rad. 17 (2010) 222–226.
[29] M.V. Uz, M. Koçak, F. Lemaitre, J.C. Ehrström, S. Kemp, F. Bron, Int. J. Fatigue 31 (2009) 916–926.
[30] J. Lorthios, F. Nguyen, A.F. Gourgues, T.F. Morgeneyer, P. Cugy, Scripta Mater. 63 (2010) 1220–1223.
[31] H. Toda, E. Maire, S. Yamauchi, H. Tsuruta, T. Hiramatsu, M. Kobayashi, Acta Mater. 59 (2011) 1995–2008.
[32] J. Baruchel, J.Y. Buffiere, P. Cloetens, M. Di Michiel, E. Ferrie, W. Ludwig, E. Maire, L. Salvo, Scripta Mater. 55 (2006) 41–46.
[33] J.-Y. Buffiere, E. Maire, P. Cloetens, G. Lormand, R. Fougeres, Acta Mater. 47 (1999) 1613–1625.
[34] L. Babout, E. Maire, J.-Y. Buffière, R. Fougères, Acta Mater. 49 (2001) 2055–2063.
[35] E. Maire, A. Owen, J.-Y. Buffière, P.J. Withers, Acta Mater. 49 (2001) 143–153.
[36] E. Maire, J.C. Grenier, D. Daniel, A. Baldacci, H. Klöcker, A. Bigot, Scripta Mater. 55 (2006) 123–126.
[37] H. Matsumoto, H. Yoneda, K. Sato, T.J. Konno, S. Kurosu, D. Fabregue, E. Maire, A. Chiba, Key Eng. Mater. 436 (2010) 171–177.
[38] S. Kurosu, H. Matsumoto, A. Chiba, C. Landron, D. Fabregue, E. Maire, Scripta Mater. 64 (2010) 367–370.
[39] C.F. Martin, C. Josserond, L. Salvo, J.J. Blandin, P. Cloetens, E. Boller, Scripta Mater. 42 (2000) 375–381.
[40] C. Landron, O. Bouaziz, E. Maire, J. Adrien, Scripta Mater. 63 (2010) 973–976.
[41] E. Maire, V. Carmona, J. Courbon, W. Ludwig, Acta Mater. 55 (2007) 6806–6815.
[42] A.B. Phillion, P.D. Lee, S.L. Cockcroft, E. Maire, Metall. Mater. Trans. A 39 (2008) 2459–2469.
[43] G. Requena, P. Cloetens, W. Altendorfer, C. Poletti, D. Tolnai, F. Warchomicka, H.P. Degischer, Scripta Mater. 61 (2009) 760–763.
[44] L. Helfen, A. Myagotin, P. Pernot, M. DiMichiel, P. Mikulík, A. Berthold, T. Baumbach, Nucl. Instrum. Meth. A 563 (2006) 163–166.
[45] L. Helfen, A. Myagotin, A. Rack, P. Pernot, P. Mikulík, M. DiMichiel, T. Baumbach, Phys. Stat. Sol. (a) 204 (2007) 2760–2765.
[46] P. Cloetens, M. Pateyron-Salomé, J.Y. Buffière, G. Peix, J. Baruchel, F. Peyrin, M. Schlenker, J. Appl. Phys. 81 (1997) 5878–5885.
[47] D. Paganin, S.C. Mayo, T.E. Gureyev, P.R. Miller, S.W. Wilkins, J. Microscopy 206 (2002) 33–40.
[48] L. Helfen, T. Baumbach, P. Cloetens, J. Baruchel, Appl. Phys. Lett. 94 (2009) 104103.
[49] T.F. Morgeneyer, M.J. Starink, I. Sinclair, Acta Mater. 56 (2008) 1671–1679.
[50] Nathalie Limodin, Julien Réthoré, Jean-Yves Buffière, Anthony Gravouil, François Hild, Stéphane Roux, Acta Mater. 57 (2009) 4090–4101.
[51] A. Deschamps, L. Lae, P. Guyot, In situ small-angle scattering study of the precipitation kinetics in an Al–Zr–Sc alloy, Acta Mater. 55 (2007) 2775–2783.
[52] Xiao Pan, Xianglin Wu, Kun Mo, Xiang Chen, Jonathan Almer, Jan Ilavsky, Dean R. Haeffner, James F. Stubbins, J. Nucl. Mater. (2011), in press.
[53] P.J. Bouchard, P.J. Withers, S.A. McDonald, R.K. Heenan, Quantification of creep cavitation damage around a crack in a stainless steel pressure vessel, Acta Mater. 52 (2004) 23–34.